Improved Half-Wave Coupled V-Cavity Laser Using Aggregating-Image Multimode Interference Coupler

Qi Chen, Zhongwen Wang, Jiasheng Zhao, Jianjun Meng, and Jian-Jun He, *Senior Member, IEEE*

***Abstract*—We theoretically analyze and experimentally demonstrate improved half-wave couplers for widely tunable V-cavity lasers. An overlapping-image 6×6 MMI coupler and an aggregating-image 16×16 MMI coupler are investigated, which give optimal coupling phase and coefficient for achieving high single-mode selectivity in V-cavity lasers while producing a low loss. A single-electrode controlled tuning of 38 channels is achieved with channel spacings of 100 GHz and 150 GHz. By combining two single-electrode tuning segments at different temperatures, a wavelength tuning range of 52 channels from 1515 nm to 1585 nm is obtained, and the side mode suppression ratios (SMSRs) reach 45 dB.**

***Index Terms*—Coupled-cavity laser, half-wave coupler, multimode interference coupler, Tunable laser.**

I. Introduction

WAVELENGTH tunable lasers are key components in optical fiber communication systems and sensing applications. Over the past decades, many different types of monolithic tunable lasers have been designed and investigated. The grating-based lasers are mostly used, such as distributed feedback (DFB) laser arrays [1], [2]; sampled grating distributed Bragg reflector (SGDBR) laser [3]; digital super-mode (DS) DBR laser [4]. However, the large size and complex fabrication process of grating structures make these lasers expensive. Simpler and smaller tunable lasers have been proposed and developed since 1980's, such as the cleaved-coupled-cavity (C3) lasers [5], [6], symmetrical/asymmetrical Y-laser [7], and slotted Fabry-Perot (SFP) laser [8]. The C3 and Y-branch lasers have not been widely used in practical applications due to its poor side mode suppression ratio (SMSR), which is about 20 dB. The SFP laser can achieve satisfactory SMSR after carefully designing the width and depth of the slots between several Fabry-Perot cavities. However, the position and size of the slots need to be controlled precisely to maintain the phase relationships of each FP cavities, which influence the performance and the fabrication yield significantly [9].

More recently, V-cavity lasers (VCLs) was proposed and developed. By introducing the concept of half-wave coupler into coupled-cavity lasers, excellent single mode selectivity has been achieved theoretically and experimentally [10], [11]. V-cavity lasers fabricated on multiple quantum well (MQW) wafers have shown good lasing and tuning performance at 870 nm [12], 1310 nm [13], 1550 nm [14] and 2810 nm [15], respectively. In the C-band, 31 channels of 100 GHz spacing can be tuned digitally at a fixed temperature and ∼40 nm of wavelength tuning range can be achieved by the assistance of TEC temperature control with a good SMSR of about 38 dB [11]. In addition, quantum dots (QD) V-cavity laser has also been proposed and achieved SMSR of 35 dB for 27 channels at 1310 nm [16]. Furthermore, VCLs have the advantage of simple fabrication process, easy control algorithm and high compactness. These advantages make VCLs a promising tunable laser solution for cost-sensitive applications such as data center and optical access networks. The half-wave coupler has previously been analyzed in [10] and [17] based on a three-waveguide directional coupler and non-imaging multimode interference coupler (MMI), and the requirements on the coupling coefficient and phase of the coupler to realize optimal mode selectivity were derived based on the threshold equation of the laser.

In this paper, we analyze the half-wave coupler from the perspective of aggregating-image multimode interference (AI-MMI) coupler and optimize the half-wave coupler for V-cavity lasers. First, we analyzed the general MMI couplers, and found that an overlapping-image 6×6 MMI coupler and an aggregating-image 16×16 MMI coupler satisfy the condition of the half-wave coupler for achieving high single-mode selectivity in VCLs. Then we designed and fabricated two types of VCLs with optimized half-wave couplers. Experimental results show that the optimization of the half-wave coupler improves the SMSRs and wavelength tuning range significantly.

II. Theoretical Analysis

The V-cavity laser is composed of two Fabry-Perot cavities with slightly different lengths and a reflective multimode waveguide region, which is called the half-wave coupler. The excellent single-mode performance of the V-cavity laser is provided by this half-wave coupler, which allows the lasing mode to pass

Manuscript received May 8, 2022; revised June 3, 2022; accepted June 15, 2022. Date of publication June 20, 2022; date of current version July 7, 2022. This work was supported by the National Natural Science Foundation of China under Grant 61960206001. (*Corresponding author: Jian-Jun He.*)

Qi Chen and Zhongwen Wang are with the State Key Laboratory of Modern Optical Instrumentation, Centre for Integrated Optoelectronics, College of Optical Science and Engineering, Zhejiang University, Hangzhou 310027, China (e-mail: chenqi@ioe-zju.org; wangzhongwen@ioe-zju.org).

Jiasheng Zhao and Jianjun Meng are with Lightip Technologies Co. Ltd., 11 Xiyuan Eighth Road, C501, Hangzhou 310030, China (e-mail: jiasheng.zhao@lightip.com.cn; jianjun.meng@lightip.com.cn).

Jian-Jun He is with the State Key Laboratory of Modern Optical Instrumentation, Centre for Integrated Optoelectronics, College of Optical Science and Engineering, Zhejiang University, Hangzhou 310027, China, and also with Lightip Technologies Co. Ltd., 11 Xiyuan Eighth Road, C501, Hangzhou 310030, China (e-mail: jjhe@zju.edu.cn).

Digital Object Identifier 10.1109/JPHOT.2022.3184552

This work is licensed under a Creative Commons Attribution 4.0 License. For more information, see https://creativecommons.org/licenses/by/4.0/

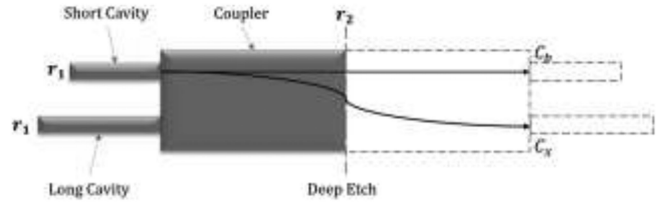

Fig. 1. Schematic diagram of the unfold half-wave coupler for V-cavity lasers.

through without loss while the side modes are suppressed. To analyze the half-wave coupler, we unfold the laser cavities with respect to the deep-etched reflecting facet of the coupler, as shown in Fig. 1. The lasing condition of the V-cavity laser can be expressed by its threshold equation [10]:

$$C_b r_1 r_2 \left[e^{2(g+ik)L} + e^{2(g'+ik')L'}\right] - \left(C_b^2 - C_x^2\right) r_1^2 r_2^2 e^{2(g+ik)L} e^{2(g'+ik')L'} = 1 \quad (1)$$

where C_b and C_x are self- and cross-coupling coefficients of the coupler, r_1 and r_2 are reflection coefficients of cavity mirrors. By calculating the threshold equation, we can obtain three required characteristics of the coupler for the best single mode selectivity. Firstly, the optimal coupling phase should be an integer multiple of π. In practical structures, π is the easiest to realize, which is the reason why it is called a half-wave coupler. Secondly, the coupling coefficient should be close to an optimal value for a given cavity length difference. Last but not least, the loss of the coupler should be as low as possible.

The half-wave coupler is essentially a section of multimode region, so we can analyze it by the theory of MMI coupler to look for certain conditions that satisfy the above three requirements.

A. General N×N MMI Coupler

The length of a general N×N MMI coupler is analyzed and calculated by guided-mode propagation analysis (MPA) method, which is [18]

$$L = \frac{p}{N} \cdot 3L_\pi \quad (2)$$

where p is an integer reflecting the periodic nature of the imaging along the multimode region and L_π is the coupling length between the two lowest-order modes, which can be written as

$$L_\pi \approx \frac{4nW^2}{3\lambda} \quad (3)$$

where n is the effective refractive index and W is the effective width of the MMI coupler. For high contrast waveguides, W can be approximated by the structural width of the MMI coupler. The light distribution at the output end face is given by [18]

$$\psi(y, L) = \frac{1}{C} \sum_{q=0}^{N-1} \psi_{in}(y - y_q) \exp(j\varphi_q) \quad (4)$$

N images with equal amplitudes numbered by q appear at the output end face, whose positions y_q and relative phases φ_q are

$$y_q = (2q - N)\frac{W}{N} \quad (5)$$

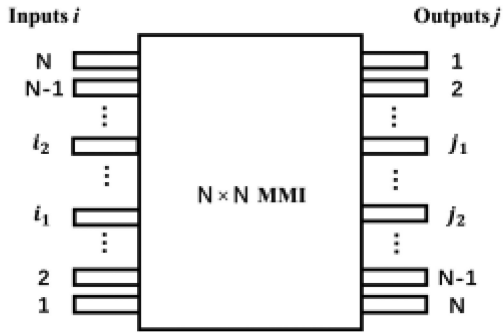

Fig. 2. Access waveguides for a N×N MMI coupler with input waveguides numbered bottom-up with index i and output waveguide numbered top-down with index j.

$$\varphi_q = (N - q)\frac{q\pi}{N} \quad (6)$$

As shown in Fig. 2, access waveguides are usually placed to receive each image. Input waveguides are numbered bottom-up with index i and output waveguide are numbered top-down with index j. The phase change from input port i to output port j is obtained from (4)

$$\varphi_{ij} = \varphi_0 + \pi + \frac{\pi}{4N} \times (j - i)(2N - j + i) \text{ for} i + j \text{ even} \quad (7)$$

$$\varphi_{ij} = \varphi_0 + \frac{\pi}{4N} \times (j + i - 1)(2N - j - i + 1) \text{ for} i + j \text{ odd} \quad (8)$$

where φ_0 is the constant phase caused by the multimode region [19]. Assuming that the two cavities of the V-cavity laser are connected to port i_1 and port i_2 in the input plane and to port j_1 and port j_2 in the output plane. The symmetry of V-cavity laser determines that $i_1 = j_1$, $i_2 = j_2$ and $i_1 + i_2 = j_1 + j_2 = N + 1$. When the light is incident from port i_1 or port i_2, the relative phase difference between port j_1 and port j_2 is

$$\Delta\varphi = \left(\frac{N}{4} - 1\right)\pi \text{ if} N \text{ is even} \quad (9)$$

$$\Delta\varphi = \frac{\pi}{4N}[N^2 - (2i - 1)^2] \text{ if} N \text{ is odd} \quad (10)$$

For couplers with single mode selectivity, the relative phase difference should satisfy $\Delta\varphi = l \cdot \pi (l = 0, 1, 2 \ldots)$, which means

$$N = 4(l + 1) \text{ if} N \text{ is even} \quad (11)$$

$$N = 2l + \sqrt{(2l)^2 + (2i - 1)^2} \text{ if} N \text{ is odd} \quad (12)$$

When N is even, it should be an integer multiple of 4. The actual coupler for V-cavity laser should be a more compact structure, so l generally takes the minimum value of 0, which means $N = 4$. Take the case of $i = 1$ as an example, when light enters the input port 1, the relative phase difference between images of the output port 1 and port 4 is 0. The lasing mode in this case is in phase when entering the coupler and can pass through without loss, which is shown in Fig. 3(a) calculated by FDTD.

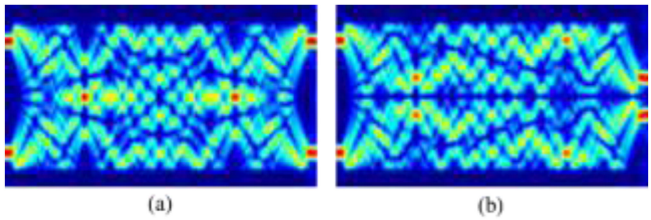

Fig. 3. Light distribution of a 4×4 MMI coupler when (a) in-phase and (b) 180°-out-of-phase modes are incident into port 1 and port 4.

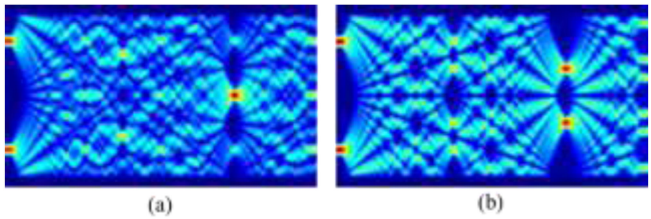

Fig. 4. Light distribution of a 9×9 MMI coupler when (a) in-phase and (b) 180°-out-of-phase modes are incident into port 2 and port 8.

While the side modes with phase difference deviated from 0 would suffer from varying degrees of loss. Fig. 3(b) shows the worst case that all the power is scattered from the middle of the output ports when the input lights are 180° out of phase. Since this is a general 4×4 MMI coupler, the self-coupling coefficient and cross-coupling coefficient are both 0.5, which correspond to the optimal value for a cavity length difference of 30% based on the threshold equation. The loss of the lasing mode in the coupler can be described as [10]

$$\varepsilon = 10\log_{10}\left[|C_b|^2 + |C_x|^2 + 2\,|C_b|\cdot|C_x|\cdot|\cos(\Delta\varphi)|\right] \tag{13}$$

where $\Delta\varphi$ is the coupling phase of the coupler. Therefore, the general 4×4 MMI coupler is a lossless coupler for the lasing mode.

When N is odd, both l and i should be 2 to ensure that N is the smallest integer value, which is 9. For a 9×9 MMI coupler with light entering the input port 2 or port 8, the relative phase difference between images of the output port 2 and port 8 is 2π. The lasing mode in this case is also in-phase when entering the coupler. As shown in Fig. 4, although the coupler achieves a coupling phase of 2π, it cannot guarantee that the light of the lasing wavelength is completely coupled into the output waveguide, and there is a non-negligible loss. Since this is a general 9×9 MMI coupler, the self-coupling coefficient and cross-coupling coefficient are both 0.33. The loss of the lasing mode is calculated to be 3.6 dB from (13). Therefore, the 9×9 MMI coupler is not a suitable coupler for V-cavity laser.

B. Overlapping-Image 6×6 MMI Coupler

When the input waveguide is specifically set at mW/N (m = 0,1,2 …N), the generally separated images on the output end face would overlap in pairs, resulting in a reduced number of images at the output of MMI couplers. The new images are numbered top-down with index k. This type of coupler is called

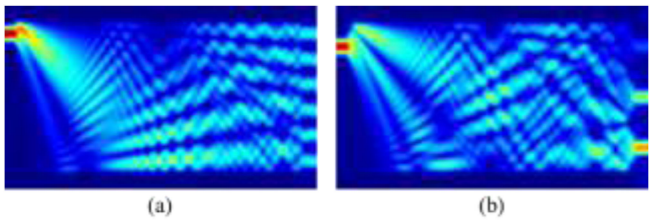

Fig. 5. Light distribution of a general 6×6 MMI coupler with input waveguide (a) Not specifically selected and (b) at 5*W*/6.

TABLE I
SIX IMAGES OF AN OVERLAPPING-IMAGE 6×6 MMI COUPLER WITH INPUT WAVEGUIDE AT 5*W*/6

Port *j*	6	5	4	3	2	1
Position	W/6	W/6	W/2	W/2	5W/6	5W/6
Amplitude	$1/\sqrt{6}$	$1/\sqrt{6}$	$1/\sqrt{6}$	$1/\sqrt{6}$	$1/\sqrt{6}$	$1/\sqrt{6}$
Phase/rad	π	5π/6	11π/6	4π/3	3π/2	7π/3

TABLE II
INTERFERENCE RESULTS OF AN OVERLAPPING-IMAGE 6×6 MMI COUPLER WITH INPUT WAVEGUIDE AT 5*W*/6

Port *k*	3	2	1
Position	W/6	W/2	5W/6
Amplitude	0.7887	0.5774	0.2113
Phase/rad	11π/12	-5π/12	-π/12

overlapping-image MMI coupler and can still be treated by the theory of the general MMI coupler [20]. Based on the interference principle, the intensity and phase of the overlapped images are obtained from the addition of their complex amplitudes

$$E = \frac{1}{\sqrt{N}}\exp(i\varphi_1) + \frac{1}{\sqrt{N}}\exp(i\varphi_2) \tag{14}$$

where φ_1 and φ_2 are the relative phases of the overlapping images.

Here we analyze the overlapping-image 6×6 MMI coupler with input waveguides at *W*/6 or 5*W*/6. The size of a typical InP-based 6×6 MMI is 8.6 μm×102 μm from (2) and (3). For cases where the input waveguide position is not specifically selected, six images are shown clearly at the end face, which is shown in Fig. 5(a). When light enters the input waveguide located at 5*W*/6, the positions and relative phases of the six images calculated by (4) is shown in Table I. Six images with amplitude of $1/\sqrt{6}$ are located at *W*/6, *W*/6, *W*/2, *W*/2, 5*W*/6 and 5*W*/6. Their relative phases are π, 5π/6, 11π/6, 4π/3, 3π/2 and 7π/3, respectively. By adding the complex amplitudes of the overlapping images, the number of images decreases to three with new amplitudes and relative phases, as shown in Fig. 5(b) and Table II. The relative phase difference between the output port 1 and port 3 is π, their amplitudes are 0.2113 and 0.7887. By introducing a total internal reflection (TIR) structure of 90° angle to swap the coupling coefficient of output port 1 and port 3 [21], the

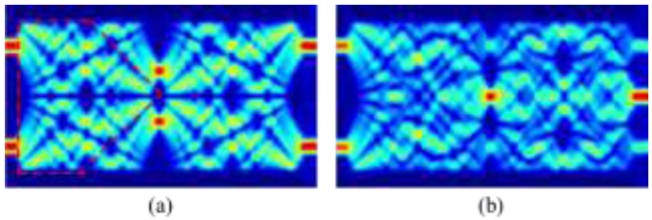

Fig. 6. Light distribution of an overlapping-image 6×6 MMI coupler with input/output waveguides at W/6 and 5W/6 when (a) 180°-out-of-phase and (b) in-phase modes are incident into port 1 and port 3. Red dashed line is a half-wave MMI coupler with a total internal reflection structure of 90° angle.

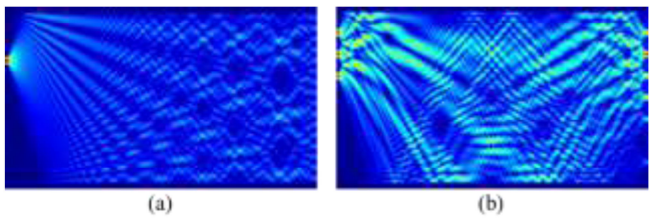

Fig. 7. Light distribution of a 16×16 MMI coupler with input waveguides (a) Not specifically selected and (b) at 5*W*/8, 3*W*/4 and 7W/8 simultaneously.

overlapping-image 6×6 MMI coupler with input waveguides at *W*/6 and 5*W*/6 will be a lossless coupler with coupling phase of π and self-coupling coefficient of 0.7887, which is an optimal lossless half-wave coupler for VCLs with 8.5% cavity length difference.

The input modes in this case are out of phase with a phase difference of π. For the lasing mode, constructive interference occurs at the output waveguides and light can pass through the coupler without loss, which is shown in Fig. 6(a). While for the side modes with phase difference deviated from π, Fig. 6(b) shows that some degree of destructive interference occurs at the output waveguides, and most of the light outputs from the middle port, which provides the single mode selectivity.

C. Aggregating-Image 16×16 MMI Coupler

We first consider a 16×16 MMI coupler with a width of 32 μm. From (2) and (3), we can obtain its length of 533 μm. When the input waveguide position is not specifically selected, sixteen images can be clearly seen at the end face, as shown in Fig. 7(a). When light enters the MMI coupler from the input waveguide located at 3*W*/4, the positions and relative phases of the sixteen images can be calculated by (4). The first and sixteenth images move to the edge and disappear, then the remaining fourteen images overlap in pairs. Finally, seven images are formed at the end face. Similarly, when light enters the MMI coupler from the input waveguides located at 5*W*/8, 3*W*/4 and 7*W*/8 simultaneously, the light distribution at the end face can be obtained by adding the complex amplitudes of the overlapped images, which is shown in Fig. 7(b). Table III gives the positions, amplitudes and relative phases of the seven overlapped images. If we further aggregate the three overlapped images at 5*W*/8, 3*W*/4 and 7*W*/8, and the three overlapped images at *W*/8, *W*/4 and 3*W*/8, by adding the complex amplitudes, we obtain the phases and amplitudes of the aggregated images as shown in Table IV.

TABLE III
IMAGING RESULTS OF A 16×16 MMI COUPLER WITH INPUT WAVEGUIDES AT 5*W*/8, 3*W*/4 AND 7*W*/8 SIMULTANEOUSLY

Port *k*	7	6	5	4	3	2	1
Position	W/8	W/4	3W/8	W/2	5W/8	3W/4	7W/8
Amplitude	0.0949	0.0327	0.1408	0.2357	0.2520	0.3318	0.2726
Phase/°	136.35	-95.59	-135.9	-56.25	-22.89	-5.63	13.9

TABLE IV
IMAGING RESULTS OF AN AGGREGATING-IMAGE 16×16 MMI COUPLER WITH INPUT WAVEGUIDE AT 3*W*/4

Port *k*	3	2	1
Position	W/4	W/2	3W/4
Amplitude	0.1848	0.2357	0.8295
Phase/°	-159.41	-56.25	-4.50

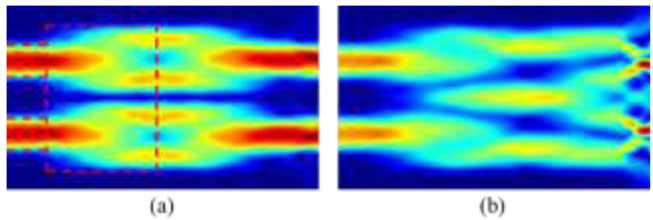

Fig. 8. Light distribution of an aggregating-image 16×16 MMI coupler with input/output waveguides at *W*/4 and 3*W*/4 when (a) 180°-out-of-phase and (b) in-phase modes are incident into port 1 and port 3. Red dashed line is a reflective half-wave MMI coupler with deep-etched facet.

The 16×16 MMI coupler is reduced to a 3×3 coupler with a relative phase of 154.91° and amplitude ratio of 4.5 between port 1 and port 3, which are close to the required characteristics of half-wave coupler for a VCL with 6% cavity length difference. To perform the aggregation, we reduce the width of the MMI to 9.4 μm, which is a typical value for a 2×2 half-wave coupler in V-cavity lasers. The length of the MMI is reduced accordingly to 46 μm based on (2) and (3). The mode field of a typical 2.5μm single-mode waveguide can cover the three images at *W*/8 spacing with the reduced-size MMI.

Then we analyze the aggregating-image MMI coupler reduced from the 16×16 MMI coupler, using the FDTD method. Only two input and output waveguides are needed at *W*/4 and 3*W*/4 for a half-wave coupler. The input modes in this case are also out of phase with a phase difference of π. For the lasing mode, as shown in Fig. 8(a), constructive interference occurs at both of the output waveguides and light can pass through the coupler with the lowest loss. While for the side modes with phase difference deviated from π, Fig. 8(b) shows that some degree of destructive interference occurs at the output waveguides, and most of the light is scattered from the middle port between the waveguides, which provides the single mode selectivity.

D. Comparison and Optimization

According to the above analysis, three types of MMI coupler with single mode selectivity are present. The first is a general 4×4 MMI coupler, whose coupling phase is 0 and coupling coefficient corresponds to the cavity length difference of 30%. The cavity length difference is often chosen to be 5% to obtain a wide wavelength tuning range and good single-mode performance at the same time. Therefore, the general 4×4 MMI coupler is not suitable for widely tunable V-cavity lasers.

The second is an overlapping-image 6×6 MMI coupler with input/output waveguides at $W/6$ and $5W/6$. This is a lossless half-wave coupler for V-cavity lasers with 8.5% cavity length difference. Its coupling phase and coupling coefficient are formed by the interference of overlapping images of the MMI.

The third is an aggregating-image 16×16 MMI coupler with input/output waveguides at $W/4$ and $3W/4$. This is a low-loss half-wave coupler whose coupling phase and coupling coefficient are close to the optimal values for cavity length difference of 6%. Its coupling phase and coupling coefficient are formed for two reasons: the interference of overlapping images and aggregation of images due to the small-size of the multimode region.

Unlike the previous design method of sweeping the parameters of the coupler over a wide range, the preliminary structural parameters of the aggregating-image half-wave coupler can be calculated analytically. Further optimizations can be performed numerically in the vicinity of those structural parameters using FDTD simulations. The aggregating-image method can therefore reduce the simulation amount significantly and help to find the best design. The theoretical loss of the optimized aggregating-image half-wave coupler for a V-cavity laser with 5% cavity length difference is only 0.18 dB, which is less than the typical value of 0.86 dB for previous half-wave couplers [10]. By fine-tuning the position of input waveguides and the size of coupler, the coupling phase and coupling coefficient can be adjusted within a small range to satisfy V-cavity lasers with various cavity length difference. However, the adjustment should not be too large, otherwise the disruption of the interference imaging conditions will result in increased losses, which means that the second and third types of half-wave MMI coupler are more suitable for V-cavity lasers with cavity length difference of about 8% and 6%, respectively.

III. Experimental Results and Discussions

Based on the overlapping-image 6×6 MMI coupler and the aggregating-image 16×16 MMI coupler, two V-cavity lasers are designed and fabricated, as shown in Fig. 9(a) and 9(b). The SEM photographs of the half-wave coupler are shown in Fig. 9(c) and (d), respectively. Since the half-wave coupler based on overlapping-image 6×6 MMI coupler has a total internal reflection (TIR) mirror, a gold coating process is only used on the deep-etched facet of the aggregating-image 16×16 MMI coupler. The cavity length differences are designed to be 5% to obtain a wide wavelength tuning range based on the Vernier effect. Theoretically, a tuning of 20 channels can be realized at a fixed temperature. The sizes of the half-wave couplers derived from the overlapping-image 6×6 MMI coupler and the

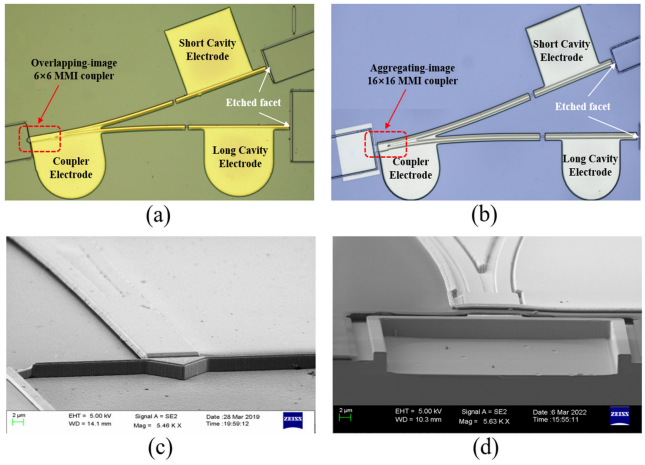

Fig. 9. Optical microscope photograph of the VCLs with (a) Overlapping-image 6×6 MMI coupler and (b) Aggregating-image 16×16 MMI coupler. SEM photograph of the half-wave couplers derived from (a) Overlapping-image 6×6 MMI coupler and (b) Aggregating-image 16×16 MMI coupler.

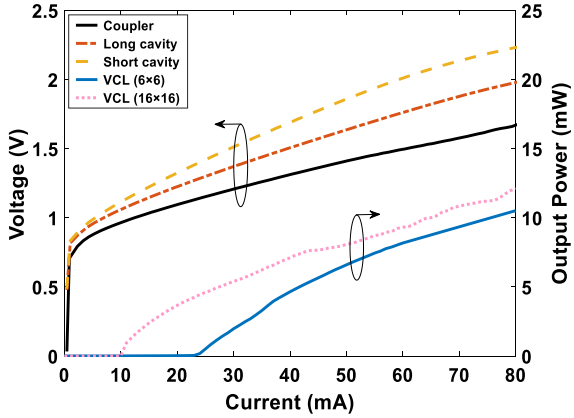

Fig. 10. IV curves of both V-cavity lasers and output power versus I_c while I_s and I_l are set to 20 mA.

aggregating-image 16×16 MMI coupler are 57×8.6 μm^2 and 25×9.4 μm^2, respectively. Coupled-cavity lasers based on the overlapping-image 6×6 MMI coupler have been investigated in [21], which obtained a tuning range of 6.5 nm with SMSR up to 40 dB. Here we optimize the parameters of the half-wave coupled V-cavity laser and obtained a larger wavelength tuning range.

The lasers are tested after being mounted on an aluminum nitride chip carrier with a thermo-electric cooler (TEC) controlled at 15°C. The light from the output port is coupled into a single mode fiber using a 3-Axis NanoMax Flexure Stages and measured by an optical spectrum analyzer (OSA) and an optical power meter. The IV curves of both V-cavity lasers are similar, which are shown in Fig. 10. The series resistances of the coupler, long cavity and short cavity are 8.7 Ω, 11.2 Ω and 12.5 Ω, respectively. The injected currents on the coupler electrode, short cavity electrode and long cavity electrode are denoted as I_c, I_s and I_l, respectively. When $I_c = 60$ mA, $I_s = 30$ mA, and $I_l = 35$ mA, the output power of both lasers measured by a large-aperture PD exceed 10 mW. The LI curves in Fig. 10 are measured by tuning I_c while I_s and I_l are set to 20 mA. The

TABLE V
COMPARISON OF PERFORMANCE METRICS FOR REPRESENTATIVE V-COUPLED-CAVITY LASERS

Authors	Wavelength (nm)	Tuning range at a fixed temperature (nm)	Extended tuning range with a varying temperature (nm)	SMSR (dB)	Power (mW)
S. Zhang [11]	1535	24	40	38	8
W. Wei [12]	870	11.4	22.4	36	22
Z. Wang [13]	1310	15	30	41.5	7
J. Meng [14]	1550	-	37	37	6
H. Yang [15]	2850	35	60	28	1.4
Y. Wan [16]	1283	4.3	-	35	9
D. D'Agostino [21]	1550	6.5	-	40	5
Stanley Cheung [22]	1330	38	-	36	3
This work	1550	50	70	45	12

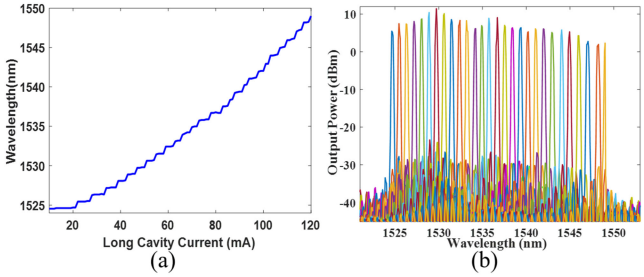

Fig. 11. Measured (a) Single-electrode wavelength tuning curve and (b) Superimposed spectra of the 28 channels of VCL based on the overlapping-image 6×6 MMI coupler with 100 GHz channel spacing at 15°C.

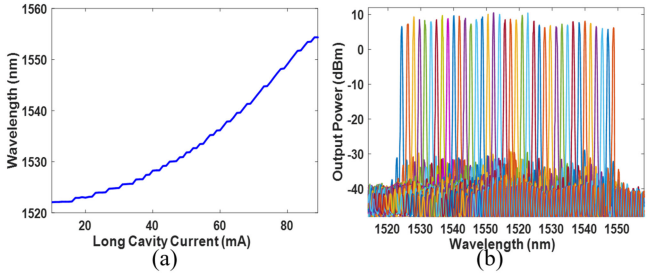

Fig. 12. Measured (a) Single-electrode wavelength tuning curve and (b) Superimposed spectra of the 38 channels of VCL based on the aggregating-image 16×16 MMI coupler with 100 GHz channel spacing at 15°C.

VCLs reach their thresholds when the currents on the coupler electrodes are 23 mA and 10 mA, respectively.

We then measured and compared the single-mode feature and tuning performance of the two lasers with 100 GHz channel spacing. Fig.11 shows the wavelength tuning curve and the corresponding superimposed spectra of the VCL based on the overlapping-image 6×6 MMI coupler. During the tuning, the temperature is fixed at 15°C, currents on the coupler electrode and short cavity electrode are 80 mA and 48 mA, respectively. Single-electrode tuning is carried out by tuning injection current on the long cavity electrode from 10 mA to 120 mA. As shown in Fig. 11(a), a discrete wavelength tuning of 28 channels from 1524.5 nm to 1549 nm is obtained, with a uniform channel spacing of about 0.875 nm or 109 GHz. The value is a little larger than the 100 GHz ITU-T grids because of the deviation between the calculated and actual group indices. This can easily be adjusted in the future design by increasing the cavity length slightly. Fig. 11(b) shows the corresponding superimposed spectra of the 28-channel wavelength tuning. The SMSRs are above 35 dB for most of the channels. The total wavelength tuning range is about 24.5 nm, which is larger than an actual FSR of 16 nm. This phenomenon is mainly caused by the red shift of material gain spectrum with the increase of chip temperature as I_1 increases. The output power varies from 11.46 dBm to 2 dBm at different channels, mainly due to the increasing temperature. The uniform power can be achieved by adjusting the injection current on the coupler electrode and short cavity electrode.

Fig. 12 shows the wavelength tuning curve and the corresponding superimposed spectra of the VCL based on aggregating-image 16×16 MMI coupler. The measurement condition is the same as above. By tuning the injection current on the long cavity electrode from 10 mA to 90 mA, as shown in Fig. 12(a), a discrete wavelength tuning of 38 channels from 1522 nm to 1554 nm is obtained, with a uniform channel spacing of about 0.84 nm or 105 GHz. The SMSRs of all the 38 channels are between 35 dB and 43 dB. The single-mode feature and tuning performance of VCL based on the aggregating-image 16×16 MMI coupler is better than that of VCL based on the overlapping-image 6×6 MMI coupler. The reason is that the half-wave coupler derived from the aggregating-image 16×16 MMI coupler with input/output waveguides at $W/4$ and $3W/4$ is more suitable for VCLs with the cavity length difference of 5%.

To study the single mode selectivity of the half-wave coupler for V-cavity lasers with different channel spacings, we also designed and fabricated the VCL based on the aggregating-image 16×16 MMI coupler with 150 GHz channel spacing. As shown in Fig. 13(a), the typical SMSR of the single mode emission reaches 45 dB. We performed a two-dimensional scanning by tuning the injected currents on the short cavity and long cavity from 0 mA to 100 mA. Fig 13(b) and 13(c) shows that the 150 GHz VCL maintains good SMSRs and high output power in a wide current range. As shown in Fig. 13(d), the injected current on the short cavity and long cavity determine the lasing wavelength together. The tuning effect of the long cavity is much better than that of the short cavity, because the wavelength tuning and the gain spectrum shift are in the same direction. By controlling the injected current on the long and short cavities cooperatively, 38 channels from 1520 nm to 1570 nm can be

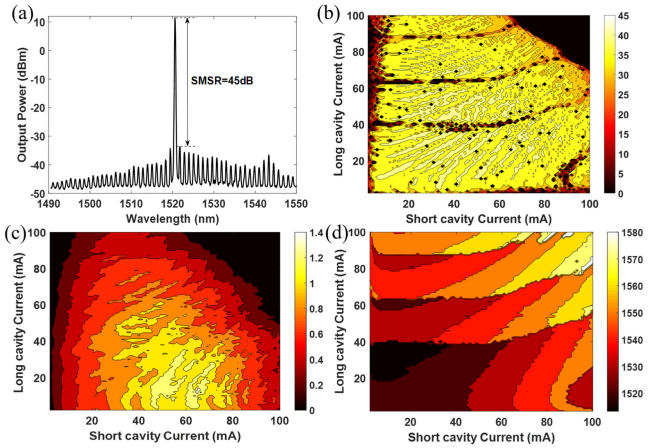

Fig. 13. Measured (a) single mode spectra with SMSR of 45 dB. Two-dimensional scanned (b) SMSRs, (c) Power and (d) wavelength of VCL based on the aggregating-image 16×16 MMI coupler with 150 GHz channel spacing at 15°C.

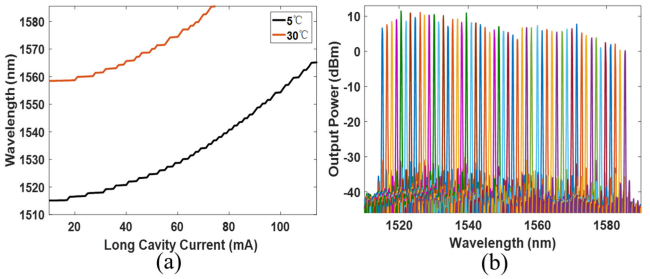

Fig. 14. Measured (a) single-electrode wavelength tuning curve and (b) Superimposed spectra of the 52 channels of VCL based on the aggregating-image 16×16 MMI coupler with 150 GHz channel spacing at 5°C and 30°C.

achieved. To further extend the wavelength tuning range, the temperature of TEC is set at 5°C and 30°C to shift the material gain spectrum. As shown in Fig. 14, a wavelength tuning of 52 channels from 1515 nm to 1585 nm is obtained. The SMSRs of most channels are over 40 dB. Table V shows the performance metrics for representative V-coupled-cavity lasers reported in previous publications. It shows that the improved half-wave coupled V-cavity laser using the aggregating-image multimode interference coupler has achieved the largest wavelength tuning range and the highest SMSR.

V. Conclusion

In conclusion, we have theoretically analyzed the half-wave couplers for V-cavity lasers by the theory of MMI coupler, and experimentally demonstrated improved VCLs. By using the concepts of aggregating-image multimode interference coupler, the half-wave coupler can be optimized for V-cavity lasers with clear physical insight. It is found that an overlapping-image 6×6 MMI coupler and an aggregating-image 16×16 MMI coupler can be used as half-wave couplers for VCLs with high single-mode selectivity. Then, we designed and fabricated two types of V-cavity lasers with half-wave couplers derived from the overlapping-image 6×6 MMI coupler with input/output waveguides at $W/6$ and $5W/6$ and the aggregating-image 16×16 MMI coupler with input/output waveguides at $W/4$ and $3W/4$, respectively. They both show good lasing and wavelength tuning performance. The improved V-cavity laser achieves a wavelength tuning range of 70 nm from 1515 nm to 1585 nm, with the SMSRs of most channels between 40 dB and 45 dB. The excellent single-mode behavior and significantly improved tuning range can further promote the V-cavity lasers for applications in DWDM communication systems and sensors.

References

[1] B. Pezeshki *et al.*, "20-mW widely tunable laser module using DFB array and MEMS selection," *IEEE Photon. Technol. Lett.,* vol. 14, no. 10, pp. 1457–1459, Oct. 2002.

[2] Z. Chung-En *et al.*, "Multiwavelength DFB laser arrays with integrated combiner and optical amplifier for WDM optical networks," *IEEE J. Sel. Topics Quantum Electron.,* vol. 3, no. 2, pp. 584–597, Apr. 1997.

[3] Y. A. Akulova *et al.*, "Widely tunable electroabsorption-modulated sampled-grating DBR laser transmitter," *IEEE J. Sel. Topics Quantum Electron.,* vol. 8, no. 6, pp. 1349–1357, Nov./Dec. 2002.

[4] N. Whitbread, "Widely tunable lasers: The digital supermode DBR," in *Proc. 16th Annu. Meeting IEEE Lasers Electro-Opt. Soc.*, 2003, vol. 2, pp. 634–635.

[5] W. Streifer, D. Yevick, T. Paoli, and R. Burnham, "An analysis of cleaved coupled-cavity lasers," *IEEE J. Quantum Electron.,* vol. 20, no. 7, pp. 754–764, Jul. 1984.

[6] J. Bowers, J. Bjorkholm, C. Burrus, L. Coldren, B. Hemenway, and D. Wilt, "Cleaved-coupled-cavity lasers with large cavity length ratios for enhanced stability," *Appl. Phys. Lett.,* vol. 44, no. 9, pp. 821–823, 1984.

[7] M. Schilling *et al.*, "Asymmetrical Y laser with simple single current tuning response," *Electron. Lett.,* vol. 28, no. 18, pp. 1698–1699, 1992.

[8] S. Mondal *et al.*, "A multiwavelength low-power wavelength-locked slotted Fabry–Perot laser source for WDM applications," *IEEE Photon. Technol. Lett.,* vol. 19, no. 10, pp. 744–746, May 2007.

[9] K. Shi *et al.*, "Characterization of a tunable three-section slotted Fabry–Perot laser for advanced modulation format optical transmission," *Opt. Commun.,* vol. 284, no. 6, pp. 1616–1621, 2011.

[10] J.-J. He and D. Liu, "Wavelength switchable semiconductor laser using half-wave V-coupled cavities," *Opt. Exp.,* vol. 16, no. 6, pp. 3896–3911, 2008.

[11] S. Zhang, J. Meng, S. Guo, L. Wang, and J.-J. He, "Simple and compact V-cavity semiconductor laser with 50 × 100 GHz wavelength tuning," *Opt. Exp.,* vol. 21, no. 11, pp. 13564–13571, 2013.

[12] W. Wei, H. Deng, and J.-J. He, "GaAs/AlGaAs-based 870-nm-band widely tunable edge-emitting V-cavity laser," *IEEE Photon. J.,* vol. 5, no. 5, Oct. 2013, Art. no. 1501607.

[13] Z. Wang, Q. Chen, Z. Fan, and J.-J. He, "Tunable V-cavity laser based on half-wave multimode interference reflector in O-band," in *Proc. Semicond. Lasers Appl. X*, Bellingham, WA, USA, vol. 11545, 2020, Art. no. 1154509.

[14] J. Meng *et al.*, "Full C-band tunable V-cavity-laser based TOSA and SFP transceiver modules," *IEEE Photon. Technol. Lett.,* vol. 29, no. 12, pp. 1035–1038, Jun. 2017.

[15] H. Yang, R. Q. Yang, J. Gong, and J.-J. He, "Mid-infrared widely tunable single-mode interband cascade lasers based on V-coupled cavities," *Opt. Lett.,* vol. 45, no. 10, pp. 2700–2703, 2020.

[16] Y. Wan *et al.*, "Directly modulated single-mode tunable quantum dot lasers at 1.3 μm," *Laser Photon. Rev.,* vol. 14, no. 3, 2020, Art. no. 1900348.

[17] X. Lin, D. Liu, and J.-J. He, "Design and analysis of 2 × 2 half-wave waveguide couplers," *Appl. Opt.,* vol. 48, no. 25, pp. F18–F23, Sep. 2009.

[18] L. B. Soldano and E. C. Pennings, "Optical multi-mode interference devices based on self-imaging: Principles and applications," *J. Lightw. Technol.,* vol. 13, no. 4, pp. 615–627, 1995.

[19] M. Bachmann, P. A. Besse, and H. Melchior, "General self-imaging properties in N × N multimode interference couplers including phase relations," *Appl. Opt.,* vol. 33, no. 18, pp. 3905–3911, 1994.

[20] M. Bachmann, P. Besse, and H. Melchior, "Overlapping-image multimode interference couplers with a reduced number of self-images for uniform and nonuniform power splitting," *Appl. Opt.,* vol. 34, no. 30, pp. 6898–6910, 1995.

[21] D. d'Agostino, D. Lenstra, H. Ambrosius, and M. Smit, "Coupled cavity laser based on anti-resonant imaging via multimode interference," *Opt. Lett.,* vol. 40, no. 4, pp. 653–656, 2015.

[22] S. Cheung, "High-speed, directly-modulated widely tunable 1310 nm coupled cavity laser via multimode interference," *J. Lightw. Technol.,* vol. 37, no. 9, pp. 2133–2139, 2019.